Systematic pathway generation and sorting in martensitic transformations: Titanium α to ω

D. R. Trinkle,[1,2] D. M. Hatch,[3] H. T. Stokes,[3] R. G. Hennig,[2] and R. C. Albers[4]
[1]*Materials and Manufacturing Directorate, Air Force Research Laboratory, Wright Patterson Air Force Base, Dayton, Ohio 45433-7817, USA*
[2]*The Ohio State University, Columbus, Ohio 43210, USA*
[3]*Brigham Young University, Provo, Utah 84602, USA*
[4]*Theoretical Division, Los Alamos National Laboratory, Los Alamos, New Mexico 87545, USA*
(Received 11 January 2005; published 5 July 2005)

Martensitic phase transitions appear in a diverse range of natural and engineering material systems. Examination of the energetics and kinetics of the transformation requires an understanding of the atomic mechanism for the transformation. A systematic pathway generation and sorting algorithm is presented and applied to the problem of the titanium α to ω transformation under pressure. The transformation pathways are separated into strain and shuffle components. All pathways are constructed within energetically motivated strain and shuffle constraints, and efficiently sorted by their energy barriers. The geometry and symmetry details of the seven lowest energy barrier pathways are given. The lack of a single simple geometric criterion for determining the lowest energy pathway shows the necessity of atomistic studies for pathway determination. The general algorithm can determine the pathway for any martensitic transformation.

DOI: 10.1103/PhysRevB.72.014105 PACS number(s): 61.50.Ks, 05.70.Fh, 64.70.Kb, 81.30.Kf

I. INTRODUCTION

Structural phase transformations govern a wide range of material properties. For example, the presence of martensitic phase transformations is responsible for the behavior of material systems as diverse as steels,[1] shape-memory alloys,[2] and planetary cores.[3] Martensitic transformations are first-order, diffusionless, displacive, athermal crystal structure transformations. A displacive transformation deforms the lattice and changes the shape of the crystal, while the diffusionless nature requires the relative motion of the atoms to be small compared to the nearest-neighbor distances.[4] Understanding the atomic mechanism for such transformations is required for examining both the energetics and kinetics of the transformation.[5]

The lattice deformation of martensitic transformation results in characteristic orientation relationships: Specific vectors and planes in the initial lattice are transformed to specific vectors and planes in the final lattice. The orientation relations can be measured experimentally for many materials and provide constraints on the possible atomistic pathways of the transformation. However, martensitic transformations proceed near the speed of sound, complicating a direct observation of the atomic motion.[1] Despite these conditions on the atomic motion, the atomistic pathway for many martensitic transformations—the precise motion of each atom during the transformation—remains unknown.

An important example is the martensitic transformation of titanium's room temperature α phase (hcp) to the high-pressure ω phase (three-atom hexagonal cell) at approximately 2–9 GPa.[6] This transformation lowers toughness and ductility in Ti alloys. Like all martensitic transformations, $\alpha \rightarrow \omega$ is a fast transformation with small atomic displacements, so that experiments[7–12] can only provide some limits on possible mechanisms; moreover, without a systematic algorithm for generation, it is impossible to determine the lowest energy barrier pathway. These problems meant that the mechanism for the $\alpha \rightarrow \omega$ transformation was only recently elucidated by Trinkle *et al.*[13] In addition, this pathway provided a necessary starting point for the study of the suppression of the $\alpha \rightarrow \omega$ transformation in alloys by impurities.[14]

The problem of finding the most likely pathway for a transformation reduces to generating a relevant subset of possible pathways and sorting them by their energy barriers. There are infinitely many unique ways to transform one crystal continuously into another. Only a finite subset of these pathways, however, results in small strain and small atomic motion. Our "pathway generation and sorting" algorithm produces the set of pathways with small total shape change (strain) and small atomic motion (shuffle). From this set, we use the energy barrier of each transformation pathway to determine the most likely pathway. The pathway generation is related to the symmetry-based method of characterizing martensitic phase transitions called COMSUBS.[15,16]

To apply the pathway generation and sorting algorithm to Ti $\alpha \rightarrow \omega$, we proceed in several steps. Section II begins by describing the notation used. We divide the pathway generation problem into two steps: Section III determines the strains for each pathway and then Sec. IV determines the internal relaxations needed for each pathway. Finally, Sec. V combines the pathway generation methods with the energy barrier evaluation methods into a general algorithm for producing all relevant pathways and sorting by energy barrier, and applies it to the problem of the Ti $\alpha \rightarrow \omega$ transformation.[13] Section VI discusses the geometry, symmetry, and energy barriers of the seven lowest-energy barrier pathways. The general and systematic pathway generation and sorting algorithm is applicable to other displacive, diffusionless transformations.

II. BACKGROUND

A. Definition of pathway

A *pathway* between two infinite periodic crystals **a** and **b** is a reversible mapping between the atoms in crystal **a** and **b**. Once each atom in **a** is identified with an atom in **b** we continuously transform from one crystal into another; moreover, the position of each atom during this transformation is calculated to determine the energy barrier of the transformation. We separate the problem of finding mappings between the endpoints—"pathway generation"—from following the transformation from **a** to **b** to determine the *energy barrier* for finding the lowest energy pathway. Once energy barriers are known, we choose the lowest energy barrier pathway: the "sorting" of the pathways.

Pathways for martensitic phase transformations can be separated into *strain*—a global shape change, and *shuffle*—small atomic relaxations. The strain results in a macroscopic change of lattice vectors $\vec{a}_i$. The shuffles produce changes in the atomic basis x_j.

We restrict ourselves to the mappings that are periodic for the entire transformations. This restricts us to homogeneous pathways from infinite crystal **a** to **b**. By enforcing periodicity, we consider only certain transformation strains. The shuffles for each pathway are periodic; this periodicity allows for a finite search of possible pathways. Enforcing homogeneity makes the homogeneous energy barrier the relevant "figure of merit" for each pathway.

We scale the volumes of our crystals so that the volume per atom in **a** is equal to that in **b**. This simplifies the calculation of the strain. For an appreciable volume change, a volumetric strain can be added to the resulting pathways.

B. Notation

A crystal **a** has lattice vectors written as a matrix $[a]$ of column vectors. The volume of the unit cell is $\det[a]$; moreover, the lattice vectors $\{\vec{a}_i\}$ are linearly independent: $\det[a] \neq 0$. The atomic basis vectors x_j are column vectors in unit cell coordinates; we can represent all Cartesian points in the infinite lattice using integer column vectors k, $\vec{R}(k;j) = [a](x_j+k)$. In general, $[a]$ and $[b]$ will represent the lattice vectors of crystals **a** and **b**, respectively; we will also use $[a]$ to denote the lattice.

A *sublattice* $[A]$ of a lattice $[a]$ is a lattice wherein every point in $[A]$ is also in $[a]$. The lattice vectors $[A]$ are called the *supercell*. In order for $[A]$ to be a sublattice of $[a]$, there must exist a nonsingular integer matrix $[n]$ such that $[A] = [a][n]$. This condition guarantees that any point in $[A]$ is also a point in $[a]$. The *size* of the supercell $[A]$ is the ratio of the number of points in $[a]$ to $[A]$; it is $\det[n]$. Generally, we will write $[A]$ and $[B]$ for a supercell of $[a]$ and $[b]$, respectively; the integer matrix $[n]$ will relate $[a]$ to $[A]$, and $[m]$ will relate $[b]$ to $[B]$.

Atoms in crystal **a** are mapped into new positions in the crystal **A**. The basis for **A** is $\{u_i^a\}$; each atom in **A** is identified with some atom in **a**: $[A]u_i^a = [a](x_j+k)$, where k is a column vector of integers. This means that $u_i^a = [n]^{-1}(x_j+k)$ for some integer vector k. We require that each component of u_i^a be in $[0,1)$, so that there are exactly $\det[n]$ possible vectors k. This means that if **a** has N_a atoms, then **A** will have $N_a \det[n]$ atoms.

A *pathway* is described as a supercell pair $[A]$ and $[B]$ with N atom positions u_i and shuffles δ_i. Each supercell relates to its crystal by $[A](u_i) = [a](x_j^a+k)$ and $[B](u_i+\delta_i) = [b](x_j^b+k') + (\text{constant shift})$, where k and k' are integer vectors and the constant shift is a uniform translation of every point in the lattice. These equations connect the atom positions u_i and shuffles δ_i to the underlying crystals **a** and **b**. Moreover, the supercells $[A]$ and $[B]$ are related by a symmetric strain tensor ε and a rotation matrix Φ, as

$$\varepsilon[A] = \Phi[B]. \tag{1}$$

The strain ε changes the lattice vectors $[A]$ into those of $[B]$ after a rotation. This corresponds to a change in the lattice vectors $[a]$ since $[A]=[a][n]$. Moreover, the strain is determined *entirely* by the supercells.

These equations allow us to write each *pathway* as $P([n],[m];u_i,\delta_i)$, where $[A]=[a][n]$ and $[B]=[b][m]$. The advantage of working in terms of the integer matrices $[n]$ and $[m]$ is the convenience in enumerating all possible supercells of interest. We will often talk about a *supercell pair* $[n]$ and $[m]$ and write $P([n],[m];*)$ to indicate that atom positions and shuffles have not yet been determined for this pathway.

We determine the strain, orientation relations, distance that atoms move, distance of closest approach to other atoms, and common subgroup from $P([n],[m];u_i,\delta_i)$. The strain ε is determined purely by the supercell pair $P([n],[m];*)$. The *orientation relations*—which vectors and planes in the lattice $[a]$ are transformed into vectors and planes in the lattice $[b]$—are also determined from $P([n],[m];*)$. The shuffle information is sufficient to determine a continuous linear simultaneous transformation from **a** to **b**; we use this transformation to calculate the distance that each atom moves and the distance of closest approach.

We determine whether two pathway representations P and P' are different by comparing their supercell pairs and their shuffles. At each step, equivalent pathway representations are removed. The details of these comparisons are in Sec. III C for the supercell pairs and Sec. IV D for the shuffles.

III. SOLVING THE STRAIN PROBLEM

The first step in enumerating possible pathways is to find the set of supercell pairs $P([n],[m];*)$. We find all supercell pairs of a given size N where the strain ε is limited by a cutoff $\varepsilon_{\max}$. We begin by enumerating possible unique sublattices of a given size, and reduce this list by the lattice symmetry. We then revisit Eq. (1) and solve for the strain ε and rotation Φ. We restrict strains to a cutoff $\varepsilon_{\max}$ to produce a finite search algorithm enumerating all possible supercell pairs. Some aspects of this problem were originally considered in Lomer's calculation of the orientation relations in U $\beta \rightarrow \alpha$.[17]

A. Unique sublattices

We say that two lattices **x** and **y** with lattice vectors $[x]$ and $[y]$, respectively, are *equivalent* if every point in $[x]$ is a point in $[y]$ and vice versa. This mirrors the definition of the sublattice from Sec. II B; i.e., $[x]$ and $[y]$ are equivalent if and only if $[x]$ is a sublattice of $[y]$ and $[y]$ is a sublattice of $[x]$. This means there are two nonsingular integer matrices $[i]$ and $[j]$ such that $[x]=[y][i]$ and $[y]=[x][j]$. Combining these equations shows that $[i]$ and $[j]$ must be *unimodular*; that is, $\det[i]=\pm 1$ and $\det[j]=\pm 1$. This gives another condition for equivalence: There exists an integer unimodular matrix $[l]$ such that $[x]=[y][l]$.

We can apply this definition to supercells as well; two supercells, given by $[n]$ and $[n']$ are equivalent if and only if there exists an integer unimodular matrix $[l]$ such that $[n]=[n'][l]$. This also means that equivalent supercells must be of the same size; i.e., $|\det[n]|=|\det[n']|$. We use unimodular matrices to iterate over possible supercell representations for a sublattice; this is equivalent to forming alternate supercells that have the same size.

From each set of equivalent supercells, we pick one representative called $[\bar{n}]$; all other members of the set can be generated using integer unimodular matrices $[l]$ as $[\bar{n}][l]$. The representative sublattices are given by an upper-triangular matrix $[\bar{n}]$, where $\bar{n}_{ij}\geqslant 0$ for all i,j, $\bar{n}_{ij}<\bar{n}_{ii}$ for $j>i$, and $\Pi_{i=1}^{d}\bar{n}_{ii}=N$, where N is the size of the sublattice $\det[\bar{n}]$. It is straightforward to show that for a given N there is a finite set of supercells in this form. If two matrices $[\bar{n}]$ and $[\bar{n}']$ have the above form, they are equivalent if and only if they are equal (see Appendix D of [18]).

Using the form for representative supercells we enumerate all possible unique sublattices for $[a]$ and $[b]$. The set of unique sublattices for $[a]$ is $\{[\bar{n}]\}$ and for $[b]$ is $\{[\bar{m}]\}$. We restrict ourselves to pathways of a given size N; this requires that $N_a\det[\bar{n}]=N=N_b\det[\bar{m}]$, where N_a and N_b are the number of atoms in crystal **a** and **b**, respectively.

To further reduce the set of representative supercells, consider the set of all symmetry operations G_a on $[a]$ where at least one lattice point is mapped to itself; this is the *point group* of **a**. We can represent each member of the point group G_a with a matrix g_a that operates on the Cartesian coordinates of $[a]$. In order to be a symmetry element, g_a must map the lattice $[a]$ back onto itself: There exists an integer unimodular matrix $\bar{g}_a$ such that $g_a[a]=[a]\bar{g}_a$. Since the lattice **a** is left invariant under the operation of g_a, two initially *different* sublattices **A** and **A**' may be *equivalent* by g_a.

To determine the set of equivalent sublattices of size N for a given lattice **a**, we start with the set of unique representations $\{[\bar{n}]\}$ and reduce it by symmetry. We say that two of our (initially unique) representations $[\bar{n}]$ and $[\bar{n}']$ are equivalent if there exists a symmetry element g_a (with integer unimodular matrix $\bar{g}_a$) and some integer unimodular matrix $[i]$ such that $\bar{g}_a[\bar{n}]=[n']=[\bar{n}'][i]$. Thus, our initial list of unique sublattices of size N may be further reduced by the symmetry of lattice **a**. Such a reduction can also be applied to the sublattices of lattice **b**.

B. Calculating and limiting the strain

Given two sets of sublattice representatives $\{[\bar{n}]\}$ and $\{[\bar{m}]\}$ for **a** and **b**, respectively, we find all strains that transform from one sublattice into the other. We limit the allowed strain by a maximum cutoff $\varepsilon_{\max}$, which produces a finite list of possible supercell pairs. We begin by solving the strain equation (1) for the general case. We then limit the allowed strain, and translate that limit into a subset of allowed supercell pairs.

We take a supercell representative $[\bar{n}]$ for **a** and $[\bar{m}]$ for **b** and substitute into Eq. (1) to get an equation for the possible strains from $[\bar{n}]$ to $[\bar{m}]$. The supercells are $[A]=[a][\bar{n}][i]$ for some integer unimodular matrix $[i]$, and $[B]=[b][\bar{m}][j]$ for some integer unimodular matrix $[j]$. The equation for ε and Φ is $\varepsilon[a][\bar{n}][i]=\Phi[b][\bar{m}][j]$, which can be simplified by right multiplying by $[i]^{-1}$,

$$\varepsilon[a][\bar{n}]=\Phi[b][\bar{m}][l], \tag{2}$$

where $[l]=[j][i]^{-1}$ is an integer unimodular matrix.

To find all possible strains, we will solve Eq. (2) for all integer unimodular matrices $[l]$ to find the supercell pairs $P([\bar{n}],[\bar{m}][l];*)$. We right multiply Eq. (2) by $[\bar{n}]^{-1}[a]^{-1}$ to get $\varepsilon=\Phi[b][\bar{m}][l][\bar{n}]^{-1}[a]^{-1}$. We define the matrix $C([l])=[b][\bar{m}][l][\bar{n}]^{-1}[a]^{-1}$; then $\varepsilon=\Phi C([l])$. The strain tensor ε is symmetric, though $C([l])$ and Φ are not. We left multiply each side of the equation by its transpose to get

$$\varepsilon^{\mathrm{T}}\varepsilon=C([l])^{\mathrm{T}}\Phi^{\mathrm{T}}\Phi C([l]),$$

$$\varepsilon^2=C([l])^{\mathrm{T}}C([l]), \tag{3}$$

where the second equality is true because ε is symmetric and Φ is a rotation matrix, so that $\Phi^{\mathrm{T}}=\Phi^{-1}$. Thus, ε is the square root of $C([l])^{\mathrm{T}}C([l])$, a symmetric matrix. We calculate the square root by diagonalizing $C([l])^{\mathrm{T}}C([l])$ and writing it as $\Theta c\Theta^{\mathrm{T}}$, where Θ is a rotation matrix and c is a diagonal matrix of the eigenvalues. Then, $\varepsilon=\Theta\sqrt{c}\Theta^{\mathrm{T}}$, and $\sqrt{c}$ are the diagonal strain elements of ε; because there is no volumetric change, the product of the diagonal strain elements are unity. Once ε is known, $\Phi=\varepsilon[a][\bar{n}][l]^{-1}[\bar{m}]^{-1}[b]^{-1}$. This method may also be considered an extension of the method of magic strains.[19]

Although every integer unimodular matrix $[l]$ has an associated strain tensor ε, most of these will be large. We define a strain limitation in terms of the cutoff $\varepsilon_{\max}>1$; a strain ε is within our cutoff if for all nonzero vectors $\vec{v}$,

$$\varepsilon_{\max}^{-1}|\vec{v}|\leqslant|\varepsilon\vec{v}|\leqslant\varepsilon_{\max}|\vec{v}|. \tag{4}$$

This condition is equivalent to requiring that all the eigenvalues of our strain matrix are between $\varepsilon_{\max}^{-1}$ and $\varepsilon_{\max}$. We consider only those $[l]$ that will produce a strain within our $\varepsilon_{\max}$ cutoff.

Equation (1) relates each supercell lattice vector $\vec{A}_i$ to a supercell lattice vector $\vec{B}_i$; this translates Eq. (4) to a condition on each $\vec{B}_i$. We substitute $\vec{A}_i$ for $\vec{v}$ in Eq. (4), noting that $\varepsilon\vec{A}_i$ is $\vec{B}_i$, so that for each i,

$$\varepsilon_{\max}^{-1}|\vec{A}_i|\leqslant|\vec{B}_i|\leqslant\varepsilon_{\max}|\vec{A}_i|. \tag{5}$$

Thus, if $\{\vec{B}_i\}$ does not satisfy Eq. (5), then ε will *never* satisfy Eq. (4). Hence, only $\vec{B}_i$ which lie in the annulus between $\varepsilon_{\max}^{-1}|\vec{A}_i|$ and $\varepsilon_{\max}|\vec{A}_i|$ need to be considered; this is a finite list for each $\vec{B}_i$.

We translate Eq. (5) into a condition on the allowed unimodular integer matrices $[l]$. For each i, we construct the (finite) set of integer vectors $\{\lambda_j^{(i)}\}$ such that $B_i=[b][\bar{m}]\lambda_j^{(i)}$ satisfies Eq. (5). This set will be different for each i, as well as for each supercell $[\bar{n}]$ and $[\bar{m}]$. To construct all of the possible unimodular matrices $[l]$, we check to see if the matrix $[l(j_1,j_2,j_3)]=(\lambda_{j_1}^{(1)}\lambda_{j_2}^{(2)}\lambda_{j_3}^{(3)})$ has determinant 1. If it does, we determine ε for the supercells $[\bar{n}]$ and $[\bar{m}][l(j_1,j_2,j_3)]$, and make sure that ε is within the cutoff $\varepsilon_{\max}$. To efficiently construct the $\{\lambda_j^{(i)}\}$ we choose representations $[\bar{n}]$ and $[\bar{m}]$ that have the *shortest* possible lengths in Cartesian coordinates for unit cells $[a]$ and $[b]$, respectively. This makes $|\vec{A}_i|$ as short as possible for each $[\bar{n}]$, and makes the set of $\lambda_j^{(i)}$ to check as small as possible.

C. Uniqueness of supercell pairings

Two different supercell pairs $P([\bar{n}],[\bar{m}][l];*)$ and $P([\bar{n}'],[\bar{m}'][l'];*)$ are equivalent if they produce the same mapping from **a** to **b**. This first requires that $[\bar{n}]=[\bar{n}']$ and $[\bar{m}]=[\bar{m}']$ since supercell representatives are equivalent if and only if they are equal. However, $[l]$ and $[l']$ need not be equal to give equivalent mappings if they produce equivalent strains from **a** to **b** and vice versa.

Two strains ε and ε' on a crystal **a** are *equivalent* if for arbitrary elastic constants C_{ij}^a the elastic energies $U_a(\varepsilon)$ and $U_a(\varepsilon')$,

$$U_a(\varepsilon)=\frac{1}{2}\sum_{i,j=1}^{6} C_{ij}^a e_i e_j,$$

are equal. The strains e_i are related to the strain matrix ε by

$$\varepsilon=\begin{pmatrix} 1+e_1 & \frac{1}{2}e_6 & \frac{1}{2}e_5 \\ \frac{1}{2}e_6 & 1+e_2 & \frac{1}{2}e_4 \\ \frac{1}{2}e_5 & \frac{1}{2}e_4 & 1+e_3 \end{pmatrix}.$$

The symmetry of the elastic constants C_{ij}^a is given by the class[20] of **a**; there are 11 unique three-dimensional crystal classes, and five unique two-dimensional crystal classes. We perform the same test for the strains on crystal **b**. This test takes into account the point group symmetry of the lattices **a** and **b**.

As an example, consider the cubic crystal class; it has only three unique elastic constants C_{11}, C_{12}, and C_{44}. We write the energy for a general strain e_i as

$$U_a(\varepsilon)=\frac{1}{2}C_{11}(e_1^2+e_2^2+e_3^2)+C_{12}(e_1e_2+e_2e_3+e_3e_1)+\frac{1}{2}C_{44}(e_4^2+e_5^2+e_6^2).$$

To determine if two strains are truly identical, we check that the three combinations $e_1^2+e_2^2+e_3^2$, $e_1e_2+e_2e_3+e_3e_1$, and $e_4^2+e_5^2+e_6^2$ are the same for ε and ε'. Similar expressions can be derived for the other crystal classes.

IV. DETERMINING SHUFFLES

Each supercell pair $P([n],[m];*)$ represents the strain of the transformation; to complete the pathway description requires knowledge of the local atomic motion: the atom positions u_i and shuffles δ_i. We find the shuffles using a systematic approach to enumerate all possible mappings between the atoms in the supercell $[A]$ and the atoms in $[B]$. We use geometric restrictions to reduce the set of possible pathways to those that require small atomic motions and do not have artificially small approach distances during the transformation.

A. Populating cells

For a given supercell pair $P([n],[m];*)$, we populate the $[A]$ supercell with the atoms from **a** and the $[B]$ supercell with the atoms from **b** using the formula from Sec. II B. The atom positions u_i^a in $[A]$ are $u_i^a=[n]^{-1}(x_j^a+k)$ for some integer vector k; similarly, $u_i^b=[m]^{-1}(x_j^b+k')$. We restrict all of the components of u_i^a and u_i^b to be in $[0,1)$, so that there are exactly N atoms from each crystal.

The shuffle vectors δ_i connect u_i^a to the atoms u_j^b in the periodic supercell as the strain ε connects $[A]$ to $[B]$. Because of the periodicity of the supercells, the mapping can connect an atom i to any periodic image of an atom j that is not inside the original supercell. Suppose we have our mapping, and each u_i^a is transformed into some $u_{j(i)}^b+h_j$ where h_j is an integer vector; our shuffle vectors are $\delta_i=u_{j(i)}^b+h_j-u_i^a$.

Our problem then is to find the mapping for each atom i in $[A]$ to an atom j in $[B]$. Moreover, we remove mappings that result in large atomic motions or bring two atoms close together, both of which produce large energy barriers.

B. Center of mass

We require that the shuffles do not change the center of mass (COM) of the crystal during the transformation: $\Sigma_i\delta_i=0$. This is enforced by shifting all of the atoms u_j^b by a constant vector δ_{COM}. Then, $\delta_i=u_{j(i)}^b+\delta_{\mathrm{COM}}+h_j-u_i^a$. We solve for δ_{COM} by summing δ_i over all N atoms:

$$\sum_i \delta_i=0=\sum_i (u_{j(i)}^b+\delta_{\mathrm{COM}}+h_j-u_i^a),$$

$$=\sum_j u_j^b-\sum_i u_i^a+N\delta_{\mathrm{COM}}+\sum_j h_j.$$

Then

$$\delta_{\mathrm{COM}} = \frac{1}{N}\sum_i (u_i^a - u_i^b) - \frac{1}{N}\sum_j h_j.$$

The only term in this equation that depends on the specific mapping is the sum over integer vectors h_j. Thus, every center of mass shift δ_{COM} has the form

$$\delta_{\mathrm{COM}} = \frac{1}{N}\sum_i (u_i^a - u_i^b) + \frac{1}{N}(k_1,k_2,k_3), \tag{6}$$

where $k_i=0\ldots N-1$. We need not consider shifts larger than this, as shifts by integer vectors only translate all of the atoms u_i^b from one periodic supercell image to another.

Because every mapping will have a center of mass shift given by Eq. (6), we systematically attempt each shift δ_{COM} on the atoms u_j^b, and make the mappings from u_i^a to u_j^b keeping only those where $\Sigma_i\delta_i=0$. We still consider mappings where u_i^a moves to $u_j^b+h_j$, but restrict the h_j components to all be either -1, 0, or 1. This prevents an atom from moving across an entire supercell.

The N^3 center of mass shifts δ_{COM} are reduced by considering only shifts that stay within the unit cell of **a** and **b**. There are some shifts k/N where $[m]k/N$ is all integer; this corresponds to shifting all of the atoms in **b** by a lattice vector of $[b]$. This will create no unique pathways, but rather previously considered pathways with a permutation of the atom indices j. Similarly, some shifts correspond to shifting all of the atoms by a lattice vector of $[a]$; these need not be considered either. We reduce the set of possible δ_{COM} to those that are within a single unit cell of $[a]$ (defined by $[n]$) and $[b]$ (defined by $[m]$). Depending on the orientation of $[n]$ and $[m]$, this reduces the number of center of mass shifts to somewhere between $N^3/(N_aN_b)$ and $N^3/\max(N_a,N_b)$.

C. Mapping atoms for a given center of mass shift

For each supercell pair $P([n],[m];*)$, we loop over the set of possible center of mass shifts δ_{COM} and enumerate all possible mappings for each center of mass shift. This becomes a combinatoric problem; to reduce the exponential scaling, we examine only mappings where no atom moves "far," given by a shuffle cutoff $\delta_{\max}$. We further reduce the set of possible mappings to those where atoms do not approach closely and where the total shuffle for all atoms is small.

We define a metric $d(x-y)$ between two vectors x and y in supercell coordinates

$$d(x-y) = \sqrt{\frac{1}{2}|[A](x-y)|^2 + \frac{1}{2}|[B](x-y)|^2}. \tag{7}$$

This distance function is symmetric in the supercells $[A]$ and $[B]$, is zero if and only if $x=y$, and obeys the triangle inequality. We use this function to compare the atom positions u_i^a and u_j^b even though they are defined from different supercells; only pathways where all atoms move less than $\delta_{\max}$ are considered.

Given our distance function, we calculate the distance $d(u_j^b+h-u_i^a)$ for all i and j and shifts h. We construct the possible shifts h for each i and j on a component-by-component basis to minimize the number of h's to consider. If the lth component of $u_j^b-u_i^a$ is less than 0, we use $h_l=0$ or $h_l=1$; if instead it is greater than 0, we allow $h_l=0$ or $h_l=-1$. In this way, we construct 2^3 shifts h for each pair i,j. This produces a table of N by $8N$ entries of distances.

For each atom i we construct the set of atoms $C(i)=\{u_j^b+h\}$ where each atom is within $\delta_{\max}$ of u_i^a. These are the allowed atom identifications for each i. Our combinatorial problem is on the sets $C(i)$; no two atoms i and i' may map to the same atom j. The set of possible pathways is found by iteration, performed using recursion. For $i=1$, we pick in turn one element of $C(1)$; this will be $j(1)$. For each $i>1$, we remove any entries of $j(1)$ from $C(i)$; call the new sets $C_{(1)}(i)$. We then pick in turn one element of $C_{(1)}(2)$; this is $j(2)$. For each $i>2$, we remove any entries of $j(2)$ from $C_{(1)}(i)$; call the new sets $C_{(1,2)}(i)$. We repeat for successive i until $i=N$, at which point we have an entire mapping $j(i)$. If at any point a set $C_{(1,\ldots,k)}(i)$ for $i>k$ becomes empty or we exhaust all the possible entries in a set, we go back and make a different choice for some smaller i. This will produce all possible mappings consistent with the initial sets $C(i)$.

After each possible pathway is constructed, we calculate the δ_i and only keep pathways where $\Sigma_i\delta_i$ is zero. Because we consider all possible δ_{COM} in our "outer loop," we are guaranteed to enumerate all possible pathways within our $\delta_{\max}$ limit. We store the possible pathways for each center of mass shift, and then check that each pathway is unique.

D. Uniqueness of pathways

Because each atom is indistinguishable, we define equivalence of pathways in terms of the local environment that atoms will see along the pathway. We believe our definition for equivalence is sufficient, but have not proven such. This was tested by comparing against the pathways produced in the common subgroup method.[16]

We use three tests to determine if two shuffle sets δ_i and δ_i' are equivalent. First, the sets of shuffle magnitudes must be equal:

$$\{(|[A]\delta_1|,|[B]\delta_1|),\ldots,(|[A]\delta_N|,|[B]\delta_N|)\} = \{(|[A]\delta_1'|,|[B]\delta_1'|),\ldots,(|[A]\delta_N'|,|[B]\delta_N'|)\}.$$

If this is true, then we next require that the distances of closest approach during the transformation (d_{ca}) match. We calculate d_{ca} by simultaneously linearly interpolating all atoms from their initial to final positions using a single variable x while straining the cell by $\mathbf{1}+x(\varepsilon-\mathbf{1})$. If the distance of closest approach is the same, then we check the nearest-neighbor distance for each atom in the half-strained, half-shuffled "intermediate" supercell. If those sets are the same, then we say that we have two equivalent pathways.

These tests only comprise a set of *necessary*, not sufficient, conditions for equivalence; this should not be seen as a severe limitation. First, two inequivalent paths marked as "equivalent" would be similar insofar as the transformation would produce similar local environments for the atoms. It is not entirely clear that there would be a very large difference

in energy as the crystal transformed using either pathway. Second, our choice of tests has been checked by comparing to an alternate method of atom identification using the Wyckoff positions in the strained "intermediate" lattice; both methods produced identical lists of unique pathways for many different supercell choices. While we do not know that the Wyckoff tests are not also limited, they should not have the *same* limitations, so that it is very likely that the limitations of each must be very small. Finally, the real test of equivalence is that two pathways are equivalent if for each atom in the first pathway, there is one and only one atom in the second pathway that has the same local environment during the transformation. Such a test would require a complicated $N!$ search, and would ultimately make the test for uniqueness computationally intractable. We believe our set of conditions is a useful subset of the full equivalence test.

E. Reduction by total shuffle magnitude and distance of closest approach

We remove pathways with small distances of closest approach and large rms shuffle magnitudes because their energy barriers will be high. The majority of pathways generated for a given $\delta_{\max}$ are energetically unlikely because they require two atoms to come very close together, or the majority of the atoms to move a large distance. For each supercell pair, we retain a subset of pathways by examining their rms shuffle magnitudes

$$\delta_{\mathrm{rms}} = \sqrt{\frac{1}{N}\sum_{i}^{N} d^2(\delta_i)} = \sqrt{\frac{1}{2N}\sum_{i}^{N} (|[A]\delta_i|^2 + |[B]\delta_i|^2)},$$

and the distance of closest approach for each. We find the *largest* distance of closest approach for the supercell pair $P([n],[m];*)$, and set the minimum allowed distance of closest approach to be $\min(d_{\mathrm{ca}}) = \max(d_{\mathrm{ca}}) - 0.1$ Å. For the supercell pair, the maximum allowed rms shuffle magnitude is $\max(\delta_{\mathrm{rms}}) = \max\,[\sqrt{2}\,\min(\delta_{\mathrm{rms}}),\ \delta_{\mathrm{rms}}\ (\text{best } d_{\mathrm{ca}}\ \text{pathway})]$.

These two rules (a) reject many of the poor candidates for each supercell pair, (b) while ensuring that at least one pathway for each supercell pair is examined, even if it has a small distance of closest approach. If a supercell pair has a "good" solution (small δ_{rms} and large d_{ca}) we check only a few other possible pathways; if the supercell pair does not have any "good" solutions, we check many possible pathways for that pair.

V. CALCULATING ENERGY BARRIERS

Once a set of pathways $P([\bar{n}],[\bar{m}][l];u_i,\delta_i)$ is known, we determine which pathways are the most probable for a given material. The sorting criterion we use is that the pathway with the lowest energy barrier should be the most likely to occur during a homogeneous transformation. Most martensites are believed to transform by heterogeneous nucleation, and there are some caveats involved in translating the homogeneous pathway into a heterogeneous pathway. However, those limitations are material specific, and thus cannot be solved for the general case; these issues have been addressed for titanium.[13]

Calculation of the energy barrier of a pathway requires (a) an atomic interaction potential and (b) a method for determining the energy barrier of a transformation. The latter can be solved accurately with some computational effort, or approximately with less effort. Because ultimately only the pathways with the lowest energy barriers are important and not the many higher energy pathways, we use approximate barrier calculations for the vast majority of the pathways. This leaves the accurate calculation of the barrier to a subset of the most likely pathways, reducing computational effort.

We use three methods to calculate the energy barrier, from most accurate and computationally intensive to least. The first method—the *nudged-elastic band* (NEB) method[21]—gives the accurate transformation barrier. The *landscape barrier* uses a reduced phase space of one strain and one concerted shuffle variable. The lack of relaxation makes the landscape barrier an overestimate of the nudged-elastic band barrier. The *elastic barrier* is an approximation to the landscape barrier, constructed only from the strain. The lack of atomic "stiffness" from phonons makes the elastic barrier an underestimate of the landscape barrier. Details of the landscape and elastic barriers have been published elsewhere.[18]

VI. TITANIUM $\alpha \rightarrow \omega$ RESULTS

The pathway generation and sorting algorithm was applied to the Ti $\alpha \rightarrow \omega$ transformation, and a new pathway emerged with an energy barrier lower than all others by over a factor of 4.[13] Herein we provide a detailed study of the methodology used and the remaining low energy barrier pathways studied.

A. Computational details

Parameters for the pathway generation algorithm are chosen to ensure sampling of all relevant pathways, and the total energies are computed to yield accurate energy barriers. The two-atom unit cell of hcp and three-atom unit cell of omega require that all supercell pairs contain a multiple of six atoms; thus, we use $N=6$ and 12. We require our diagonal strains be less than $\varepsilon_{\max}=1.333$; for comparison, the Burgers pathway for hcp to bcc requires a diagonal strain component of only 1.1.[22] We keep only pathways with elastic barriers less than $E_{\mathrm{cut}}=100$ meV/atom. From those supercell pairs, we construct pathways with a maximum shuffle magnitude $\delta_{\max}$ less than 2.0 Å; this is comparable to the interatomic distance in α and ω, and, as seen later, is much larger than the shuffles in our lowest energy pathway. Each supercell pair produces multiple pathways with shuffles smaller than this value. As discussed in Sec. IV E, we keep pathways with closest approach distance d_{ca} within 0.1 Å of the largest d_{ca}. We reject any pathways with an rms shuffle δ_{rms} that is larger than both the δ_{rms} of the best d_{ca} pathway found and $\sqrt{2}$ of the smallest δ_{rms}. This gives us a set of pathways with good distance of closest approach, rms shuffle, and guarantees at least one pathway for each supercell pair.

TABLE I. Number of supercell pairs, pathways generated, and cutoff parameters in Ti hcp to omega pathway search. Each consecutive step builds on the selection made in the previous step. 1. We generate an initial set of 134 supercell pairs with a given $\varepsilon_{\max}$ cutoff of 1.333. 2. We choose the 60 supercell pairs that have an elastic barrier less than E_{cut} of 100 meV/atom. 3. The possible shuffles for each supercell pair within $\delta_{\max}$ of 2 Å are determined to give 3845 possible pathways. 4. For each supercell pair, we define a minimum allowed distance of closest approach (d_{ca}), and a maximum rms shuffle magnitude (δ_{rms}), and keep the 977 pathways within those limits. 5. Finally, the seven pathways with tight-binding landscape barriers less than 90 meV/atom are kept, and their true energy barriers calculated.

	6 atom		12 atom	
Sorting step:	Supercell pairs	Pathways	Supercell pairs	Pathways
1. $\varepsilon_{\max}$	6	—	128	—
2. E_{cut}	4	—	56	—
3. $\delta_{\max}$	4	**55**	56	**3790**
4. d_{ca}, δ_{rms}	4	**6**	56	**971**
5. $E_{\text{landscape}}$	2	**2**	3	**5**

We calculate total energies for the landscape energy barriers using a tight-binding (TB) model. The TB calculations are performed using the molecular dynamics code OHMMS[23] and use Mehl and Papaconstantopoulos's functional form[24,25] with parameters refit to reproduce full-potential density-functional total energies for hcp, bcc, fcc, omega, and sc to within 0.5 meV/atom (see Appendix B of [18]). For each mechanism, we use a k-point set equivalent to a $12\times12\times9$ or $12\times12\times8$ grid in the original hcp lattice. This k-point mesh is converged to within 0.1 meV/atom against a $18\times18\times12$ k-point mesh for the three lowest energy barrier pathways. A Fermi broadening of 63 meV (5 mRyd) was used with this k-point mesh to ensure a smooth electronic density of states.

We calculate total energies and forces for the nudged elastic band barrier using carefully converged *ab initio* calculations, performed with VASP.[26,27] VASP is a plane-wave based code using ultrasoft Vanderbilt-type pseudopotentials[28] as supplied by Kresse and Hafner.[29] The calculations were performed using the generalized gradient approximation of PW91.[30] We include $3p$ electrons in the valence band and use a plane-wave kinetic-energy cutoff of 400 eV and a $7\times7\times7$ k-point mesh to ensure energy convergence to within 1 meV−atom. We relax the atomic positions and the unit cell shape and volume until the atomic forces are less than 20 meV/Å and the stresses are smaller than 20 MPa.

B. Generated pathways

Table I summarizes the resulting number of supercell pairs and pathways generated and the cutoffs made at each step in the algorithm. The nudged-elastic band energy barrier for the final seven pathways is calculated, and the pathway with the lowest barrier is TAO-1.[13]

We generate an initial set of 134 supercell pairs with diagonal strain components less than $\varepsilon_{\max}$ and reduce it to 60 pairs with elastic barriers less than E_{cut} of 100 meV/atom. The three-dimensional surface of possible diagonal strain values $\bar{\varepsilon}_i$ satisfying $\varepsilon_{\max}^{-1}\leqslant\bar{\varepsilon}_i\leqslant\varepsilon_{\max}$ and $\bar{\varepsilon}_1\bar{\varepsilon}_2\bar{\varepsilon}_3=1$ has sharp corners at the boundary; because of this, we generate more supercell pairs than are used to ensure that we produce all supercell pairs less than our elastic barrier cutoff. This procedure is analogous to inscribing a circle inside of a regular hexagon.

Using larger supercells fails to produce any supercell pairs with strains smaller than the smallest strains already found. The possibility for better pathways for larger supercell sizes is unlikely as there are no 18- or 24-atom supercell pairs found with strains smaller than the smallest strain found using 12-atom supercells. We keep the 12-atom supercell pairs because there *is* a 12-atom supercell pair that has smaller strains than the smallest strain for a six-atom pathway; three of the seven low energy pathways have this smallest strain value.[31]

The 60 supercell pairs generate 55 six-atom pathways and 3790 12-atom pathways with $\delta_{\max}$ of 2.0 Å; this set is reduced to six six-atom and 971 12-atom pathways using the closest approach distances and rms shuffle magnitudes as described in Sec. IV E. The reduction for the six-atom pathways is more severe because each of the supercell pairs has a "good" solution (small rms shuffle magnitude and large closest approach distance), so that we examine fewer alternative pathways. Many of the 12-atom supercell pairs do not have "good" solutions, so that we examine more alternative pathways. A check of this reduction for good solutions was performed by calculating the landscape barrier of the "best" excluded pathway for the TAO-1 six-atom supercell pair; it has a TB landscape barrier of 160 meV/atom, compared to 43 meV/atom for TAO-1.

The 977 pathways are then reduced to seven: three with landscape barriers less than 80 meV, and four with landscape barriers between 80 and 90 meV. The three lowest pathways are TAO-1 (six-atom), TAO-2 (six-atom), and Silcock (12-atom); the latter is a pathway already proposed in the literature.[7] The remaining six pathways are new; although TAO-1 and TAO-2 are related to Usikov and Zilberstein's $\alpha\rightarrow\beta\rightarrow\omega$ pathway through an intermediate bcc structure.[8] We calculate the nudged elastic band barrier for Silcock and TAO-1 through TAO-6.

Table II gives details for the seven lowest-barrier pathways of interest. Along each pathway, the symmetry is a subgroup of both crystals **a** and **b**. Using COMSUBS,[16] we obtained the maximal symmetry of this subgroup for each pathway. In the table, we list this maximal common subgroup along with atomic positions in the setting of this subgroup. This gives a complete description of the mapping of atoms in **a** onto atoms in **b**. For example, in the TAO-1 pathway, the symmetry of the crystal is monoclinic (space group 15 $C2/c$) as it transforms from α to ω. The atoms are at the Wyckoff (e) and (f) sites of that space group. During the transformation the atoms at the (e) site $(0,y,1/4)$ move from $(0,7/12,1/4)$ to $(0,1/2,1/4)$ and the atoms at the (f) site (x,y,z) move from $(1/3,5/12,1/2)$ to $(1/3,1/2,1/6)$.

It is important to note that in the nudged-elastic band

TABLE II. Pathways for the $\alpha \rightarrow \omega$ phase transition in Ti. Each pathway is defined by a maximal common subgroup of both the α and ω phases and Wyckoff positions. A supercell containing both phases is given in terms of the lattice vectors of α and ω unit cells; the lattice vectors determine $[n]$ and $[m]$. The atomic positions for each phase are given in the setting of the common subgroup; together the positions define u_j and δ_j. The multiplicity m for each Wyckoff position is given with the label of the position.

			Wyckoff positions			
Path	Subgroup	Supercell lattice	m	label	α	ω
TAO-1	15 $C2/c$	α:(−1,−1,2),(1,−1,0),(1,1,1)	2	(*e*)	0,7/12,1/4	0,1/2,1/4
(6-atom)		ω:(−2,−1,2),(0,−1,0),(0,0,2)	4	(*f*)	1/3,5/12,1/12	1/3,1/2,1/6
TAO-2	11 $P2_1/m$	α:(1,0,0),(0,0,1),(0,−3,0)	2	(*e*)	1/3,1/4,7/9	1/2,1/4,3/4
(6-atom)		ω:(0,0,−1),(−1,0,0),(1,2,−2)	2	(*e*)	1/3,1/4,1/9	1/3,1/4,1/12
			2	(*e*)	1/3,1/4,4/9	2/3,1/4,5/12
Silcock	57 *Pbcm*	α:(−1,0,0),(−3,−6,0),(0,0,1)	4	(*d*)	3/4,23/36,1/4	1/2,5/8,1/4
(12-atom)		ω:(0,0,1),(2,4,0),(−1,0,0)	4	(*d*)	3/4,11/36,1/4	1,7/24,1/4
			4	(*d*)	3/4,35/36,1/4	1,23/24,1/4
TAO-3	6 *Pm*	α:(1,0,0),(0,0,1),(0,−6,0)	1	(*a*)	1/3,0,1/18	0,0,0
(12-atom)		ω:(0,0,−1),(−1,0,0),(2,4,−3)	1	(*a*)	1/3,0,2/9	0,0,1/6
			1	(*a*)	1/3,0,7/18	1/2,0,1/3
			1	(*a*)	1/3,0,5/9	1/2,0,1/2
			1	(*a*)	1/3,0,13/18	1/2,0,2/3
			1	(*a*)	1/3,0,8/9	0,0,5/6
			1	(*b*)	2/3,1/2,1/9	1/4,1/2,1/12
			1	(*b*)	2/3,1/2,5/18	1/4,1/2,1/4
			1	(*b*)	2/3,1/2,4/9	5/4,1/2,5/12
			1	(*b*)	2/3,1/2,11/18	3/4,1/2,7/12
			1	(*b*)	2/3,1/2,7/9	3/4,1/2,3/4
			1	(*b*)	2/3,1/2,17/18	3/4,1/2,11/12
TAO-4	11 $P2_1/m$	α:(1,0,0),(0,0,1),(0,−6,0)	2	(*e*)	1/3,1/4,13/18	−1/8,1/4,17/24
(12-atom)		ω:(0,0,−1),(−1,0,0),(2,4,−3)	2	(*e*)	1/3,1/4,2/9	3/8,1/4,5/24
			2	(*e*)	1/3,1/4,8/9	−1/8,1/4,7/8
			2	(*e*)	1/3,1/4,1/18	7/8,1/4,1/24
			2	(*e*)	1/3,1/4,7/18	3/8,1/4,3/8
			2	(*e*)	1/3,1/4,5/9	3/8,1/4,13/24
TAO-5	6 *Pm*	α:(−1,0,0),(0,0,2),(0,3,0)	1	(*a*)	2/3,0,2/9	5/6,0,1/4
(12-atom)		ω:(0,0,1),(−2,0,0),(−1,−2,−1)	1	(*a*)	2/3,0,5/9	0,0,7/12
			1	(*a*)	2/3,0,8/9	2/3,0,11/12
			1	(*b*)	2/3,1/2,2/9	5/6,1/2,1/4
			1	(*b*)	2/3,1/2,5/9	1,1/2,7/12
			1	(*b*)	2/3,1/2,8/9	2/3,1/2,11/12
			2	(*c*)	1/3,1/4,1/9	1/2,1/4,1/12
			2	(*c*)	1/3,1/4,4/9	1/6,1/4,5/12
			2	(*c*)	1/3,1/4,7/9	1/3,1/4,3/4
TAO-6	11 $P2_1/m$	α:(1,0,0),(0,0,1),(0,−6,0)	2	(*e*)	1/3,1/4,13/18	23/24,1/4,17/24
(12-atom)		ω:(0,0,−1),(−1,0,0),(2,4,−5)	2	(*e*)	1/3,1/4,2/9	11/24,1/4,5/24
			2	(*e*)	1/3,1/4,8/9	5/8,1/4,7/8
			2	(*e*)	1/3,1/4,1/18	7/24,1/4,1/24
			2	(*e*)	1/3,1/4,7/18	1/8,1/4,3/8
			2	(*e*)	1/3,1/4,5/9	19/24,1/4,13/24

TABLE III. Comparison of lowest landscape barrier pathways. Energy barriers: Four different methods for calculating the energy barrier for the three pathways are shown, from least accurate to most accurate. The elastic barrier only accounts for the strain in each pathway. The landscape barrier uses a simple combined shuffle for each, and a tight-binding total energy. Finally, the NEB calculation is done with the tight-binding method for the lowest three and *ab initio* for all seven to accurately determine the barrier. Orientation relations: The relative orientation between α and ω is shown for each pathway.

	Silcock	TAO-1	2	3	4	5	6
Homogeneous barriers (in meV/atom)							
Elastic	3.7	18	21	3.7	3.7	21	74
TB Landscape	60	43	61	83	80	84	81
TB NEB	54	24	52	—	—	—	—
Ab initio NEB	31	9	58	32	68	37	69
Transformation information							
Supercell size	12	6	6	12	12	12	12
Orientation relations[a]	II	I	II	II	II	II	II

[a]I: $(0001)_\alpha \| (0\bar{1}11)_\omega$, $[11\bar{2}0]_\alpha \| [01\bar{1}1]_\omega$;
II: $(0001)_\alpha \| (11\bar{2}0)_\omega$, $[11\bar{2}0]_\alpha \| [0001]_\omega$.

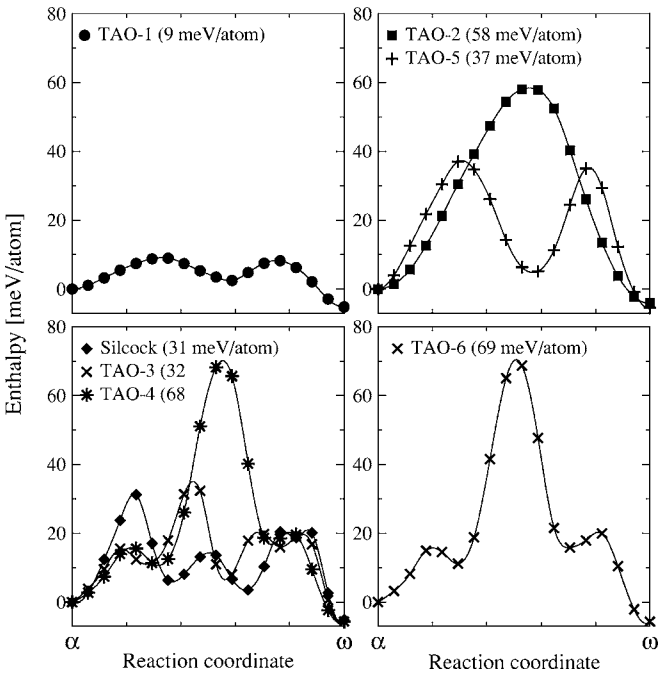

FIG. 1. Energy barrier at zero pressure for the seven lowest energy pathways, using *ab initio* NEB at 16 intermediate states. The pathways are grouped by their strains; each set has related supercell pairs. The effect of different shuffles on the energy barrier can be seen by comparing TAO-2 to TAO-5, and Silcock, TAO-3, and TAO-4 to each other. The latter three pathways have the smallest amount of strain, but the homogeneous barrier is smallest for TAO-1.

method, the atomic positions are relaxed under *triclinic symmetry*: no point symmetries are assumed or enforced. We find the resulting symmetry along each pathway to be nonetheless equal to the maximal symmetry given in Table II. In each of these cases, we conclude that the lowest barriers occur for pathways with maximal symmetry.

Table III summarizes the energy barriers and orientation relations for the seven lowest pathways of interest. The TB NEB barrier is bounded above by the landscape barrier and below by the elastic barrier. The difference between the TB NEB barrier and the *ab initio* NEB barrier is due primarily to the latter's cell size and shape relaxations. The Silcock and the TAO-2 through TAO-6 pathways all have the same orientation relations, making them indistinguishable in experiments.

Figure 1 shows the energy barrier for the seven lowest energy barrier pathways. The plots are grouped according to the supercell pairs in each pathway. The difference in energy barrier among pathways with the same supercell shows the importance of theory in understanding the microscopic mechanism—measurements of the final ω orientation relative to the α can only rule out possible pathways.

Figure 2 illustrates a simple geometric picture of the low barrier TAO-1 pathway. The basal plane of α is a series of hexagons surrounding individual atoms; these hexagons then break into two three-atom pieces. Each three-atom piece swings in opposite directions out of the basal plane, and

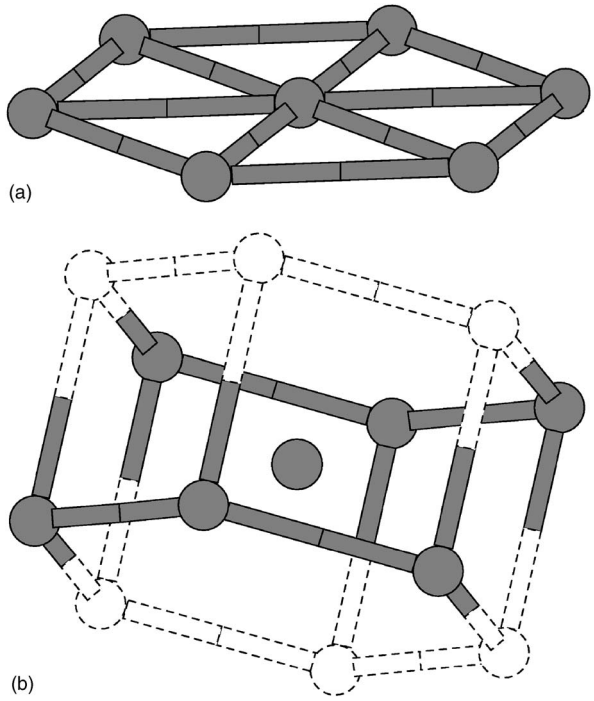

FIG. 2. TAO-1 acting on a single α basal plane. A hexagon in the basal plane is broken into two three-atom pieces. Each three-atom piece swings out of the basal plane in opposite directions, to create half of the honeycomb lattice in parallel (0001) planes of ω. The remaining atom in the center forms the *A* sublattice lying in the (0001) planes of ω. The next α basal layer creates the dashed atoms in the ω honeycomb. This transformation turns the (0001) plane of α into the $(01\bar{1}1)$ plane of ω.

connects with a mated three-atom piece above or below. These form the honeycomb sublattice of ω; the remaining "unmoved" atoms form the A sublattice in ω. This transformation transforms the (0001) plane of α into the $(01\bar{1}1)$ plane of ω.

Of the remaining six pathways, TAO-2 and Silcock are both related to existing pathways in the literature, while TAO-3 through TAO-6 are related to the other three pathways. TAO-2 has the same endpoints as Usikov and Zilberstein's variant II pathway,[8] but avoids the intermediate bcc phase. The Silcock pathway is identical to the original published pathway.[7] Both TAO-3 and TAO-4 use the Silcock supercell pairing, though with different shuffles. TAO-5 is a cell doubling of the TAO-2 supercell pairing with different shuffles. Finally, TAO-6 uses the same α supercell as Silcock, but connects it to a different ω supercell.

TAO-1 has the lowest energy barrier that best trades off between shuffle and strain. During the transformation, the closest nearest-neighbor distance is 2.63 Å, which is larger than the 2.55 Å value for TAO-2, 2.58 Å for Silcock, TAO-3, TAO-4, and TAO-6. Only TAO-5 has a comparable closest nearest-neighbor distance of 2.63 Å; this larger distance helps to explain the lower barrier compared to TAO-2 with the same strains. Because the nearest-neighbor distances in α and ω are 2.93 and 2.65 Å, respectively, it is not surprising that TAO-1 has the lowest barrier. The larger barrier of TAO-5 compared to TAO-1 may be due to more complicated geometric changes during the pathway. The lack of a simple, single criterion to explain the difference in energy barriers shows the necessity of *ab initio* studies.

VII. CONCLUSION

We have presented a general systematic pathway generation and sorting algorithm for martensitic transformations. The method enumerates all possible pathways within a few geometric restrictions. When applied to the Ti $\alpha \rightarrow \omega$ transformation, a previously unknown pathway emerges with a barrier much lower than all other pathways. Geometric criteria are useful in reducing the large set of possible pathways to a more manageable set, but *ab initio* studies are required to ultimately find the lowest energy barrier pathway. The general and systematic pathway generation and sorting algorithm is applicable for finding the pathway for any displacive, diffusionless transformation.

ACKNOWLEDGMENTS

We thank J. W. Wilkins for helpful discussions. D. R. T. thanks Los Alamos National Laboratory for its hospitality and acknowledges support from the Fowler Fellowship at The Ohio State University. This research is supported by DOE grants DE-FG02-99ER45795 (OSU), DE-FG02-03ER46059 (BYU), and W-7405-ENG-36 (LANL). Computational resources were provided by the Ohio Supercomputing Center and NERSC.

[1] *Martensite*, edited by G. B. Olson and W. S. Owen (ASM, Metals Park, OH, 1992).
[2] *Shape Memory Materials*, edited by K. Otsuka and C. M. Wayman (Cambridge University Press, 1998).
[3] L. Vočadlo, D. Alfè, M. Gillan, I. Wood, J. P. Brodholt, and G. D. Price, Nature (London) **424**, 536 (2003).
[4] P. Haasen, *Physical Metallurgy*, third ed., translated by J. Mordike (Cambridge University Press, Cambridge, UK, 1996).
[5] G. B. Olson and M. Cohen, Metall. Trans. A **7**, 1897 (1976).
[6] S. K. Sikka, Y. K. Vohra, and R. Chidambaram, Prog. Mater. Sci. **27**, 245 (1982).
[7] J. M. Silcock, Acta Metall. **6**, 481 (1958).
[8] M. P. Usikov and V. A. Zilbershtein, Phys. Status Solidi A **19**, 53 (1973).
[9] A. R. Kutsar, V. N. German, and G. I. Nosova, Dokl. Akad. Nauk SSSR **213**, 81 (1973).
[10] Y. K. Vohra, E. S. K. Menon, S. K. Sikka, and R. Krishnan, Acta Metall. **29**, 457 (1981).
[11] G. T. Gray, III, C. E. Morris, and A. C. Lawson, in *Titanium '92: Science and Technology*, edited by F. H. Froes and I. L. Caplan (Minerals Metals & Materials Society, Warrendale, PA, 1993), pp. 225–232.
[12] H. Dammak, A. Dunlop, and D. Lesueur, Philos. Mag. A **79**, 147 (1999).
[13] D. R. Trinkle, R. G. Hennig, S. G. Srinivasan, D. M. Hatch, M. D. Jones, H. T. Stokes, R. C. Albers, and J. W. Wilkins, Phys. Rev. Lett. **91**, 025701 (2003).
[14] R. G. Hennig, D. R. Trinkle, J. Bouchet, S. G. Srinivasan, R. C. Albers, and J. W. Wilkins, Nat. Mater. **4**, 129 (2005).
[15] H. T. Stokes and D. M. Hatch, Phys. Rev. B **65**, 144114 (2002).
[16] H. T. Stokes and D. M. Hatch, ISOTROPY software package, http://stokes.byu.edu/isotropy.html (2004).
[17] W. M. Lomer, in *The Mechanism of Phase Transformations in Metals*, in Institute of Metals Monograph and Report Series no. 18 (The Institute of Metals, London, 1956), pp. 243–252.
[18] D. R. Trinkle, Ph.D. thesis, Ohio State University, 2003.
[19] B. W. Van de Waal, Acta Crystallogr., Sect. A: Found. Crystallogr. **46**, FC17 (1990).
[20] J. F. Nye, *Physical Properties of Crystals* (Clarendon, Oxford, 1957).
[21] H. Jónsson, G. Mills, and K. W. Jacobsen, in *Classical and Quantum Dynamics in Condensed Phase Simulations* edited by B. J. Berne, G. Ciccotti, and D. F. Coker (World Scientific, Singapore, 1998), p. 385.
[22] W. G. Burgers, Physica (Utrecht) **1**, 561 (1934).
[23] J. N. Kim, OHMMS home page, http://www.mcc.uiuc.edu/ohmms.
[24] M. J. Mehl and D. A. Papaconstantopoulos, Phys. Rev. B **54**, 4519 (1996).
[25] M. J. Mehl and D. A. Papaconstantopoulos, Europhys. Lett. **60**, 248 (2002).
[26] G. Kresse and J. Hafner, Phys. Rev. B **47**, R558 (1993).
[27] G. Kresse and J. Furthmüller, Phys. Rev. B **54**, 11169 (1996).
[28] D. Vanderbilt, Phys. Rev. B **41**, R7892 (1990).

[29] G. Kresse and J. Hafner, J. Phys.: Condens. Matter **6**, 8245 (1994).

[30] J. P. Perdew, in *Electronic Structure of Solids '91* edited by P. Ziesche and H. Eschrig (Akademie Verlag, Berlin, 1991), pp. 11–20.

[31] It is worth noting that the lowest energy pathway does have a larger strain than the smallest strain found, but it is also a six-atom pathway.